Thermophysics and Aeromechanics, *2019*, *Vol. 26*, *No. 5*

DOI: 10.1134/S0869864319050019

Determination of the laminar-turbulent transition location in numerical simulations of subsonic and transonic flows past a flat plate*

A.V. Boiko[1,2], K.V. Demyanko[1,3], A.A. Inozemtsev[4], S.V. Kirilovskiy[1], Yu.M. Nechepurenko[1,3], A.P. Paduchev[4], and T.V. Poplavskaya[1]

[1]*Khristianovich Institute of Theoretical and Applied Mechanics SB RAS*, *Novosbirsk*, *Russia*

[2]*University of Tyumen*, *Tyumen*, *Russia*

[3]*Marchuk Institute of Numerical Mathematics RAS*, *Moscow*, *Russia*

[4]*UEC Aviadvigatel*, *Perm*, *Russia*

E-mail: boiko@itam.nsc.ru, popla@itam.nsc.ru

(*Received April 11*, *2019*; *revised May 20*, *2019*;
accepted for publication June 4, *2019*)

The study is aimed at determining the position of the laminar-turbulent transition in subsonic and transonic two-dimensional boundary layers with the use of a novel software package LOTRAN 2.0 developed by the authors. The package is based on the e^N-method and employs numerical data of numerical simulations of the laminar flow performed by standard gas-dynamic software systems based on the Reynolds-averaged Navier–Stokes equations. As an example, the flow past a flat plate is considered. The good agreement of the computed and experimental data on the laminar-turbulent transition location is demonstrated. New data on the laminar-turbulent transition in the boundary layer on a flat plate for transonic flow regimes are obtained.

Keywords: numerical simulation, subsonic and transonic flows, laminar-turbulent flow, laminar-turbulent transition, LTT module.

Introduction

The cost efficiency of flying vehicles depends to a large extent on the ratio of the lengths of the laminar and turbulent parts of the boundary layer and on the length of the laminar-turbulent transition (LTT). Other conditions being identical, the laminar flow is preferable. The LTT process also exerts a significant effect on flow separation and heat transfer in the boundary layer, which largely determines the requirements to various structural elements of the flying vehicle and to localization of equipment. Therefore, the determining factor of adequate simulation of the flow around flying vehicles is a correct computation of the LTT position and

* This work was financially supported by the Russian Science Foundation (Grant No. 18-19-00460).

length. If they are computed incorrectly, there may be significant errors, e.g., in determining the drag force of the vehicle.

Both specialized software products [1–3] and general gas-dynamic CFD software, in particular, the ANSYS Fluent system [4], are widely used for solving various problems of heat and mass transfer. Various approaches based on LTT prediction can be used for modeling the laminar-turbulent flow within the framework of the Reynolds-averaged Navier–Stokes (RANS) equations implemented into such software systems. At the moment, the most popular empirical model for LTT prediction in academic research and industry is the model developed in [5], where two additional differential equations (for intermittency and Reynolds number of the transition beginning based on the momentum loss thickness) are added to two transport equations of the k-ω SST turbulence model (for the turbulent kinetic energy and specific rate of turbulent energy dissipation); moreover, the model is closed only by empirical relations.

The LTT model implemented in ANSYS Fluent was called "Transition SST." It includes three proprietary dependences derived for subsonic flows. The model [5] can be implemented in various software systems: in the modern commercial CFD system STAR-CCM+, version 3.0 [6], DLR TAU code actively used in German aerospace industry [7], and in the RANS code elsA (ONERA) specially developed for turbine flows [8, 9]. It should be noted that the Transition SST model in all CFD systems mentioned above was calibrated only for subsonic incompressible flows; therefore, this LTT model requires validation for transonic and supersonic flows [10]. Moreover, the presence of proprietary dependences significantly constrains applications of this LTT model.

Currently there are specialized industrial software systems that accurately reproduce the propagation of small perturbations in comparatively simple flows. They are aimed at computing the LTT position in the boundary layer based on criteria of reaching certain threshold amplitude (e^N-method). The most well-known systems are the Graphical Transition Prediction Toolkit (GTPT) [11] and NOnLOcal Transition analysis (NOLOT) [12]. The wide use of this approach in aerodynamic applications is caused by the fact that it is based on a physically grounded linear theory of hydrodynamic stability, which is valid for both two-dimensional and three-dimensional incompressible and compressible flows up to hypersonic velocities if the free-stream turbulence level is sufficiently low as, e.g., in flight conditions or in test sections of quiet wind tunnels. It should be also noted that this method is still under development for more complex flows [13–15].

In 2013, the authors of the present paper developed and registered a LOTRANxx software package for computing the LTT position in boundary layers of viscous incompressible fluid flows past low-curvature surfaces [16, 17]. Then much effort was applied for further development of this software package for computing the LTT position in compressible boundary layers [18], resulting in the development of two new packages called LOTRAN 2.0 and LOTRAN 3.0, which are designed for basic academic research of stability of two-dimensional and three-dimensional boundary layers of viscous compressible flows, respectively, and for determining the LTT position by the e^N-method.

The present paper describes the operation of the LOTRAN 2.0 package combined with the ANSYS Fluent 18.0 CFD software for computing subsonic and transonic laminar-turbulent flows past a flat plate. Comparisons are performed of 2D and 3D results with each other, with available experimental data found in non-classified publications, and with results on the LTT position computed by LOTRAN 2.0 and the Transition SST model. These comparisons were aimed not only at verification of numerical data against experimental results, but also at determination of the area of applicability of the Transition SST model and e^N-method for flows in the considered range of Mach numbers, in particular, for transonic flow regimes.

1. Numerical simulation of the laminar flow

The laminar flow without perturbations was computed by means of solving two-dimensional Navier–Stokes equations with the use of the ANSYS Fluent CFD software. Numerical simulations of a 2D gas flow on a flat plate with a blunted leading edge were performed for subsonic and transonic velocities of the external flow. The model had the following parameters: length of 3 m and leading edge bluntness radius of 0.3 mm (Fig. 1*a*). The fluid was air under normal conditions at a zero altitude above the sea level.

The computational domain consisted of a rectangle and a quarter of a circle with a radius of 7 m; the plate was located at the center of the lower boundary (Fig. 1*a*). The x distance from the trailing edge of the plate to the output boundary was 7 m. This size of the computational domain was chosen to avoid possible influence of the domain boundaries on the computation results on the one hand and excessive reduction of the turbulence intensity on the plate surface on the other hand. As the problem implied determination of the LTT position on one side of the flat plate only, only one half of the symmetric configuration was considered for simplicity. The computational domain was divided into two subdomains: subdomain of the near-wall flow with a height of the order of several thicknesses of the boundary layer for detailed resolution of the boundary layer and satisfaction of the condition $y^+ < 1$ near the plate surface and subdomain of the far field with a coarser computational grid. The computations were performed on a block quadrangular regular grid (Fig. 1*b*) refined toward the plate surface and the leading edge (Fig. 1*a*, 1*b*). The total number of cells of the computational grid was 114000.

The two-dimensional Navier–Stokes equations were solved by using a density-based solver; an implicit scheme of the second-order accuracy in space with the Roe-FDS method

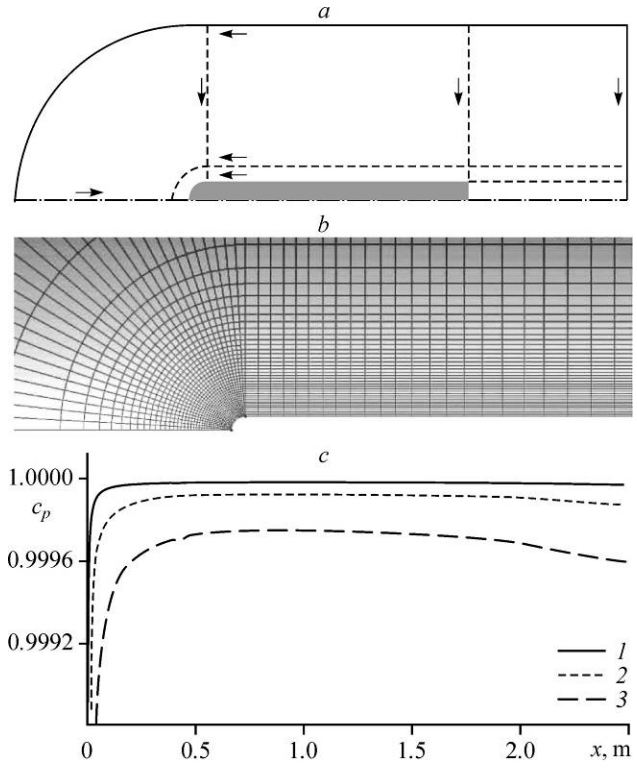

Fig. 1. Schematic image of the computational domain with division into zones and directions of grid refinement (*a*), fragment of the computational grid near the rounded leading edge of the model (*b*), and pressure distribution on the model surface for M_∞ = 0.146 (*1*), 0.3 (*2*), and 0.5 (*3*) (*c*).

Table 1

Flow parameters at constant values of $\mathrm{Re}_1 = 3.3 \cdot 10^6$ 1/m and $T_\infty = 288$ K

M_∞	U_∞, m/s	P_∞, Pa
0.146	50	98374
0.3	102	47768
0.4	136	35910
0.5	170	28700
0.6	204	23917
0.7	238	20505
0.75	255	19200
0.8	272	17945
0.85	289	16895

of convective flux splitting was used. The upper and right boundaries were subjected to the free-stream conditions, namely, p_∞, M_∞, and T_∞, which are the free-stream pressure, Mach number, and temperature, respectively (see table 1). The no-slip condition and constant temperature (T_w = 291 K) were prescribed on the plate surface; the left (upstream of the plate) and right (downstream of the plate) parts of the lower boundary of the computational domain were subjected to the symmetry condition. Computations on a sequence of nested grids showed that the solutions for the sought variables (in particular, velocity, density, pressure, and skin friction) computed on a grid with the doubled number of nodes in both directions differ by less than 1 %.

Two series of computations of the laminar compressible flow were performed for different Mach numbers M_∞ and constant unit Reynolds number Re_1 (see Table 1) and for different values of Re_1 (see Table 2). The change in the Mach number and, correspondingly, free-stream velocity for a constant unit Reynolds number was reached by changing the free-stream pressure. In the second series of computations, we had $\mathrm{Re}_1 = \dfrac{\rho_\infty c_\infty}{\mu_\infty} \cdot \dfrac{U_\infty}{c_\infty} = \mathrm{Re}_{1c_\infty} \mathrm{M}_\infty$, where the unit Reynolds number Re_{1c_∞} was calculated based on the free-stream sound velocity c_∞ (by analogy with [19]) and was constant for all computation variants, while Re_1 changed in proportion to the change in the freestream Mach number. Thus, we obtained data on the laminar boundary layers for the flat plate model (distributions of velocity, temperature, and pressure normal to the model surface). Figure 1*c* shows the pressure distributions c_p on the model surface normalized to the freestream pressure for different conditions in the external flow. It is seen that the change in pressure is less than 1 % in all cases beginning from the cross section x = 200 mm, which testifies to an almost zero streamwise pressure gradient.

Table 2

Flow parameters at variable values of Re_1 and $T_\infty = 288$ K

M_∞	U_∞, m/s	P_∞, Pa	Re_1, 1/m
0.146	50	98374	$3.3 \cdot 10^6$
0.3	102	98374	$6.78 \cdot 10^6$
0.4	136	98374	$9.041 \cdot 10^6$
0.5	170	98374	$11.3 \cdot 10^6$
0.6	204	98374	$13.56 \cdot 10^6$
0.7	238	98374	$15.82 \cdot 10^6$
0.75	255	98374	$16.95 \cdot 10^6$
0.8	272	98374	$18.08 \cdot 10^6$
0.85	289	98374	$19.21 \cdot 10^6$

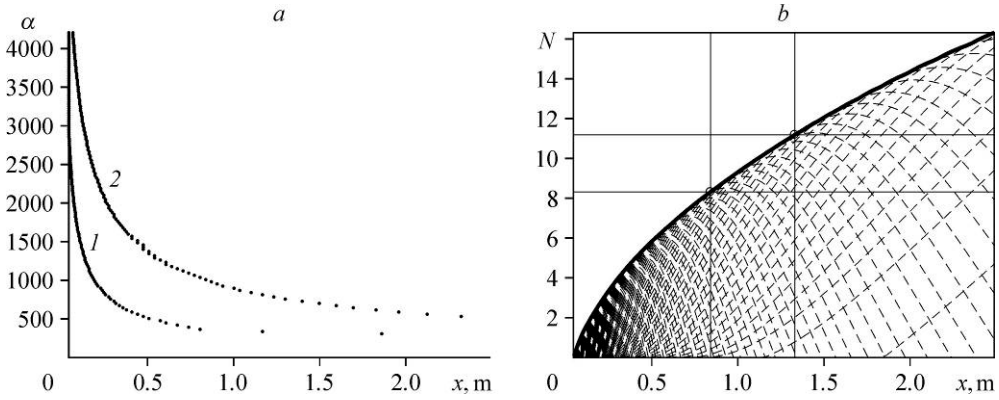

Fig. 2. Points of the onset (*1*) and breakdown (*2*) of the time instability domains (*a*), curves of *N*-factors, their envelope (black curve), threshold value of *N*-factors and LTT positions (straight lines) (*b*) computed in the course of LTT module operation. $M_\infty = 0.146$, $Re_1 = 3.3 \cdot 10^6$ 1/m, $T_\infty = 288$ K, $Tu = 0.03$ %.

2. Determination of the LTT position

The LTT position was determined by the LOTRAN 2.0 software package (in what follows, the LTT module), which involves the full three-dimensional equations of heat and mass transfer and also original specialized matrix algorithms for stability analysis. A detailed description of these equations and algorithms can be found in [18]. The data on the 2D laminar flow were converted into an internal representation of the LTT module with the use of a special data export module developed for the ANSYS Fluent CFD software. The LTT module includes multi-stage pre-processing and analysis of the boundary layer characteristics for increasing the accuracy of the subsequent stability analysis. The LTT position was determined by the e^N-method based on analyzing the growth of low-amplitude disturbances in the streamwise direction.

In the course of its operation, the module determines the boundary layer characteristics (displacement thickness, momentum thickness, surface, pressure, etc.) for qualitative evaluation of the result of assimilation of data obtained from ANSYS Fluent and shows the points of the onset (*1*) and breakdown (*2*) of the time instability domains (Fig. 2*a*), the curves of the *N*-factors, their envelope, the threshold values of the *N*-factors, and the corresponding positions of the LTT beginning and end (Fig. 2*b*).

At moderate degrees of free-stream turbulence, a typical feature of the flow on a flat plate is the transition to turbulence associated with the Tollmien–Schlichting waves [20]. Therefore, the following formulas were used for calculating the threshold values of the *N*-factors for the LTT onset (N_c) and breakdown to turbulence (N_t) [4, 20]:

$$N_c = 2.13 - 6.18 \lg Tu, \quad N_t = 5.00 - 6.18 \lg Tu \tag{1}$$

(*Tu* is the free-stream turbulence). At $Tu < 0.1$ %, it is recommended to use the threshold values of the *N*-factors [20] calculated for $Tu = 0.1$ %.

3. Comparisons of results

Results of an experimental study of the LTT on a flat plate in a subsonic flow with the free-stream turbulence of 0.03 % were reported in [21]. The LTT onset and breakdown were determined from the behavior of intermittency of the laminar and turbulent regions

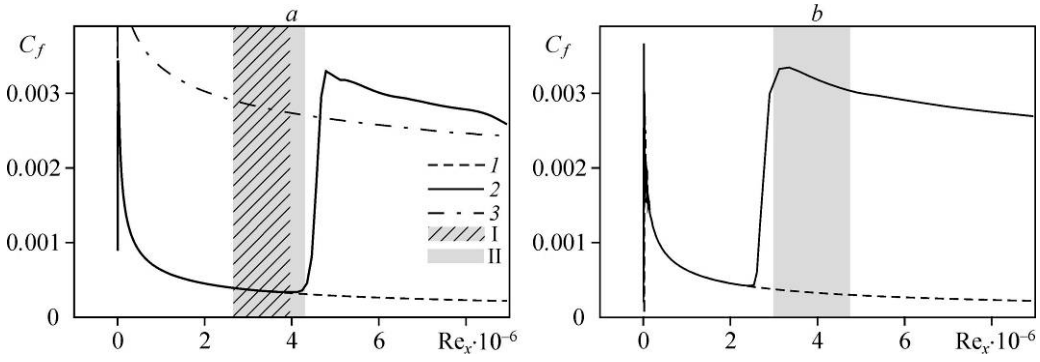

Fig. 3. Skin friction coefficients versus the Reynolds number Re_x.

a: $M_\infty = 0.146$, $Re_1 = 3.3 \cdot 10^6$ 1/m, $T_\infty = 288$ K, *b*: $M_\infty = 0.3$, $Re_1 = 6.78 \cdot 10^6$ 1/m, $T_\infty = 288$ K; *1* — data computed for the laminar flow, *2* — data computed by the Transition SST model for $Tu = 0.03$ %, *3* — data computed for the turbulent flow; regions I and II show the transition regions obtained on the basis of the experimental data [21] and computed by the LTT module (present work).

in oscillograms of the velocity fluctuations obtained by means of hot-wire measurements in the boundary layer, and the skin friction coefficients were obtained by processing the digitized profiles of the main flow velocity in the LTT region (see Fig. 3*a*). The figure also shows the computed skin friction coefficients $C_f = \tau_w \Big/ \left(2\rho_\infty U_\infty^2\right)$ (here τ_w is the shear stress, gradient of velocity along the normal, on the plate surface) as functions of the local Reynolds number $Re_x = \rho_\infty U_\infty x / \mu_\infty$, which were obtained for the flow past the plate under the same external conditions by the ANSYS Fluent software for the laminar flow regime and by the Transition SST model for the free-stream turbulence of 0.03 % with the use of the LTT module with data on the laminar flow computed by ANSYS Fluent. It is seen that the LTT region computed by the LTT module agrees well with the experimental data; the difference between the results along the streamwise coordinate is smaller than 10 %, which is a good result for modern models of the transition to turbulence. The computations by the Transition SST model demonstrate a significantly narrower LTT region than that observed in the experiments and computed by the LTT module. The difference in the values of C_f in the computations of the fully turbulent flow and by the Transition SST model in the turbulent region is apparently associated with the history of boundary layer evolution (the turbulent boundary layer starts to develop from the leading edge in the first case and only from the middle of the plate in the second case). Similar patterns are also observed in computations of the flow past the flat plate for different values of M_∞ and Re_1, as is shown in Table 2 (see Fig. 3*b*).

Figure 4 shows the skin friction coefficients C_f for transonic flow regimes computed for the laminar flow by the Transition SST model with a prescribed free-stream turbulence level of 0.03 % and by the LTT module. The predictions of the LTT module testify to a significant delay of the LTT, which is consistent with the available data on the transition to turbulence in flat-plate boundary layers at transonic velocities [22]. At the same time, the data predicted by the Transition SST model reveal an earlier LTT breakdown and a significantly smaller length of the LTT region for the transonic flow regime as compared to the data computed by the LTT module. It should be also noted that the skin friction coefficients predicted by the Transition SST model for different Mach numbers of the external flow are also identical, which contradicts the available data on the transition to turbulence on flat plates at transonic velocities [22]. This can be explained as follows: first, the Transition SST model developed for LTT computations in flows with a high degree of free-stream turbulence (in particular,

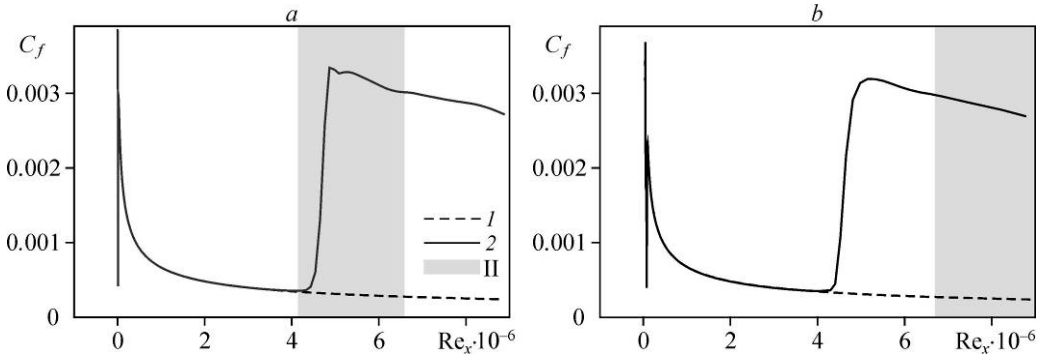

Fig. 4. Skin friction coefficients versus the Reynolds number Re_x.

a: $M_\infty = 0.5$, $Re_1 = 3.3 \cdot 10^6$ 1/m, $T_\infty = 288$ K, *b*: $M_\infty = 0.7$, $Re_1 = 3.3 \cdot 10^6$ 1/m, $T_\infty = 288$ K;
1 — data computed for the laminar flow, *2* — data computed by the Transition SST model for $Tu = 0.03$ %;
region II is the LTT region predicted by the LTT module (present work).

in the flow around turbine blades) does not provide adequate results for low-turbulence flows; second, the Transition SST model integrated into the ANSYS Fluent 18.0 software does not properly take into account the flow compressibility typical for transonic flow regimes.

Variations of the transition onset as a function of the free-stream Mach number predicted by the LTT module are shown in Fig. 5*a*. As the Mach number increases, while the unit Reynolds number remains constant, the LTT onset is first shifted downstream and the LTT region length significantly increases (see Figs. 3*a*, 3*b*, and 4). As it also follows from Fig. 5*a*, as the Mach number increases from 0.146 to 0.5 with a simultaneous increase in the unit Reynolds number, the LTT onset is naturally shifted upstream, i.e., toward the leading edge of the flat plate. With a subsequent increase in the Mach number simultaneously with an increase in the unit Reynolds number, the flow becomes turbulent immediately downstream of the leading edge of the plate. However, recalculation of the data obtained to the Reynolds number of the LTT onset Re_{x_b} shows (Fig. 5*b*) that both series of simulations yield similar results: Re_{x_b} increases with an increase in the Mach number. These data are consistent with the theoretical

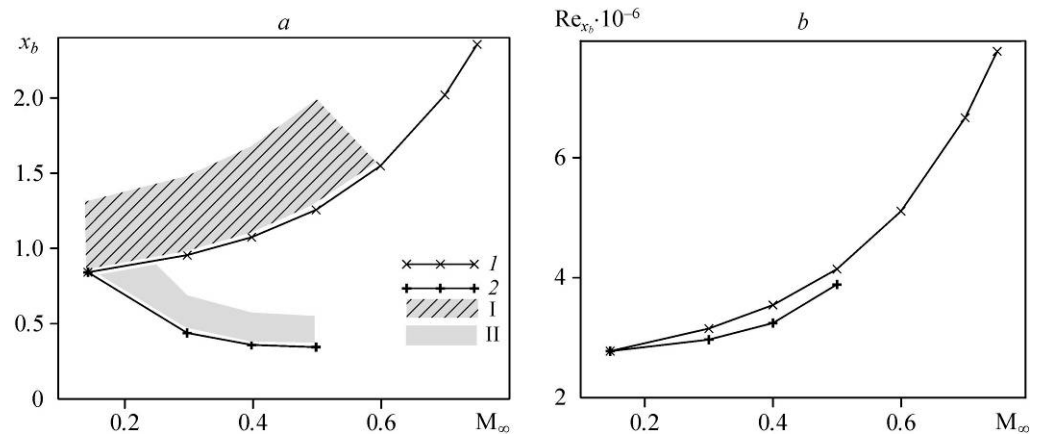

Fig. 5. Effect of the Mach number on the LTT onset (*a*)
and on the Reynolds number of LTT onset (*b*).

1 — data computed for constant Re_1 (Table 1) and LTT region I, respectively;
2 — data computed for varied Re_1 (Table 2) and LTT region II predicted by the LTT module.

calculations of the influence of the Mach number on the transition Reynolds number presented in [22], where it was demonstrated that the transition Reynolds number increases with an increase in the Mach number from zero to unity.

Conclusions

A two-dimensional laminar-turbulent flow past a flat plate at subsonic and transonic velocities of the external flow was numerically simulated with the use of a novel software package LOTRAN 2.0 based on the e^N-method. The computations were performed in the Mach number range from 0.146 to 0.75, and new data were obtained on the LTT position for a transonic flow past a flat plate at low degrees of free-stream turbulence (Tu = 0.03 %). These new results can be used for validation of the data on the transition to turbulence obtained by other numerical methods.

It was demonstrated that the LTT positions for transonic flows computed by the Transition SST model incorporated into the current versions of ANSYS Fluent are noticeably different from the data predicted by the LTT module and from the data of [22], which can be associated with the fact that flow compressibility effects are ignored in the Transition SST model integrated into the current versions of ANSYS Fluent.

Comparisons with experimental data on the LTT position in subsonic flows and with data for transonic flows available in publication [22] showed that the LOTRAN 2.0 software package is able to provide an adequate prediction of the LTT onset and breakdown; therefore, it also ensures an adequate prediction of the LTT region length in two-dimensional subsonic and transonic flows on a flat plate. In the subsonic flow considered in the present study, the error was smaller than 10 % along the streamwise coordinate. This fact also testifies that it is possible to ensure sufficient accuracy of computing the laminar boundary layer by the ANSYS Fluent CFD software for obtaining velocity profiles to be used in the LTT module developed based on the LOTRAN 2.0 software package.

References

1. **A.A. Maslov, A.N. Kudryavtsev, S.G. Mironov, T.V. Poplavskaya, and I.S. Tsyryulnikov,** Wave processes in a viscous shock layer and control of fluctuations, J. Fluid Mech., 2010, Vol. 650, P. 81–118.
2. **A.A. Maslov, A.N. Kudryavtsev, S.G. Mironov, T.V. Poplavskaya, and I.S. Tsyryulnikov,** Numerical simulation of receptivity of a hypersonic boundary layer to acoustic disturbances, J. Appl. Mech. Tech. Phys., 2007, Vol. 48, No. 3, P. 368–374.
3. **I.V. Egorov, A.V. Fedorov, and V.G. Soudakov,** Receptivity of a hypersonic boundary layer over a flat plate with a porous coating, J. Fluid Mech., 2008, Vol. 601, P. 165–187.
4. **A.V. Boiko, S.V. Kirilovskiy, A.A. Maslov, and T.V. Poplavskaya,** Engineering modeling of the laminar-turbulent transition: Achievements and problems, J. Appl. Mech. Tech. Phys, 2015, Vol. 56, No. 5, P. 30–49.
5. **F.R. Menter, R. Langtry, and S. Völker,** Transition modelling for general purpose CFD codes, Flow, Turbulence and Combustion, 2006, Vol. 77, Iss. 1–4, P. 277–303.
6. **P. Malan, K. Suluksna, and E. Juntasaro,** Calibrating the γ-Re_θ transition model for commercial CFD, AIAA Paper, 2009, No. 2009–1142.
7. **C. Seyfert and A. Krumbein,** Comparison of a local correlation-based transition model with an e^N-method for transition prediction, New Results in Numerical and Experimental Fluid Mechanics VIII: Contributions to the 17th STAB/DGLR Symposium Berlin, Germany 2010, Ed. by A. Dillmann, G. Heller, H.-P. Kreplin, et al., Springer-Verlag, Berlin, Heidelberg, 2013, P. 541–548.
8. **C. Content and R. Houdeville,** Application of the γ-Re_θ laminar-turbulent transition model in Navier–Stokes computations, AIAA Paper, 2010, No. 2010–4445.
9. **A. Benyahia, L. Castillon, and R. Houdeville,** Prediction of separation-induced transition on high lift low pressure turbine blade, ASME 2011 Turbo Expo: Turbine Technical Conference and Exposition. Heat Transfer, Parts A and B Vancouver, British Columbia, Canada, June 6–10, 2011, American Society of Mechanical Engineers, 2011, Vol. 5, P. 1835–1846.
10. **D.A. Bountin, Yu.V. Gromyko, S.V. Kirilovskiy, A.A. Maslov, and T.A. Poplavskaya,** Influence of blunt-cone tip temperature on the laminar-turbulent transition in hypersonic boundary layers, Thermophysics and Aeromechanics, 2018, Vol. 25, No. 4, P. 483–496.

11. M.R. Malik, Boundary-layer transition prediction toolkit, AIAA Paper, 1997, No. 1997–1904.
12. S. Hein, Nonlinear nonlocal transition analysis — code development and results, Recent results in laminar-turbulent transition: Selected numerical and experimental contributions from the DFG priority programme «Transition» in Germany, Ed. by S. Wagner, M. Kloker, U. Rist, Springer-Verlag, Berlin, Heidelberg, 2004, P. 123–134.
13. A.V. Boiko, A.V. Dovgal, and V.V. Kozlov, Instability of flow separation at 2D surface imperfections in a low-speed air stream (review), Thermophysics and Aeromechanics, 2017, Vol. 24, No. 2, P. 167–173.
14. A.V. Boiko, A.V. Dovgal, and A.M. Sorokin, Stability of time-periodic flow with laminar boundary-layer separation, Thermophysics and Aeromechanics, 2018, Vol. 25, No. 5, P. 667–673.
15. A.V. Boiko and Yu.M. Nechepurenko, Asymmetric self-similar flows of a viscous incompressible fluid along a right-angle corner, Thermophysics and Aeromechanics, 2018, Vol. 25, No. 2, P. 207–218.
16. A.V. Boiko, Yu.M. Nechepurenko, R.N. Zhuchkov, and A.S. Kozelkov, Laminar-turbulent transition prediction module for LOGOS package, Thermophysics and Aeromechanics, 2014, Vol. 21, No. 2, P. 191–210.
17. Yu.M. Nechepurenko and A.V. Boiko, LOTRANxx software package for computing the position of the laminar-turbulent transition in boundary layers of viscous incompressible fluid flows on surfaces with small curvature, Certificate of state registration of the computer code No. 2013660060, Russia, Rospatent (Federal Service of Intellectual Properties), 2013.
18. A.V. Boiko, K.V. Demyanko, and Y.M. Nechepurenko, On computing the location of laminar–turbulent transition in compressible boundary layers, Rus. J. Num. Anal. Math. Mod., 2017, Vol. 32, No. 1, P. 1–12.
19. V.M. Boiko and S.V. Poplavskii, Particle and drop dynamics in the flow behind a shock wave, Fluid Dynamics, 2007, No. 3, P. 433–441.
20. J.L. Van Ingen, Transition, pressure gradient, suction, separation and stability theory, AGARD-CP-224 Laminar-turbulent transition, Copenhagen, Denmark, 1977, P. 20.1–20.15.
21. G.B. Schubauer and P.S. Klebanoff, Contributions on the mechanics of boundary-layer transition, NACA TN 3489, National Advisory Committee for Aeronautic, Washington 1955.
22. L.M. Mack, Linear stability theory and the problem of supersonic boundary-layer transition, AIAA J., 1975, Vol. 13, No. 3, P. 278–289.